Non Data-Aided Carrier Tracking Techniques for Continuous-Phase Frequency-Shift Keyed Signals

Brendan Hill, Nazia Mozaffar, Salwan Damman
NIWC Pacific
53560 Hull Street, San Diego, CA 92152; 619-553-3255
brendan.hill@navy.mil

ABSTRACT

Communications between ground stations and nanosats in low earth orbit (LEO) require acquisition and tracking of large Doppler frequency offsets due to the relative velocity between the transmitter and the receiver. The Doppler frequency shift varies with time, reaching its fastest rate of change as the small satellite reaches its closest approach to the ground station. For phase modulated signals, a frequency offset estimate extracted from the band edge filters is used to correct for the Doppler shift. This approach encounters difficulties when it's used to correct for frequency offset in continuous phase frequency shift keyed (CPFSK) signals. Optimized band edge filters are designed to have a frequency response that is the derivative of the matched filter frequency response. However, CPFSK detection often requires different matched filters for different symbols, particularly when there are multiple possible magnitudes of frequency shifts to choose from in each symbol period. Having separate matched filters for different symbols complicates the effort to use optimized band edge filters as it imposes a requirement to demodulate the signal before correcting its frequency offset. Furthermore, the fact that the signal of interest is itself changing in frequency from one symbol to the next further complicates the issue. However, a modification to the classic band edge filter design can permit the detection and correction of CPFSK signals without the need to demodulate the signal. This paper presents techniques for non data-aided correction of CPFSK signals using modified matched filters in frequency locked loops (FLLs). Examples of the approaches are shown in MATLAB for varying signal-to-noise ratio (SNR), static Doppler, and dynamic Doppler.

INTRODUCTION

Small satellites in low earth orbit can close communication links to ground terminals with less power than their counterparts in higher orbits by virtue of their closer distance. Lower orbit distance translates to higher velocity, which in turn means higher Doppler frequency offset. For example, a satellite in a 500-mile altitude circular orbit above mean sea level travelling due west over Logan, Utah has a velocity of 7.45 km/s in order to stay in orbit. The satellite transmits on a 2.45 GHz carrier. A ground terminal located directly under the flight path of the satellite observes a Doppler frequency offset starting at 57kHz and gradually changing to -57kHz, as shown in Figure 1. At time t=0, the satellite is directly overhead and the ground terminal sees a 0 Hz Doppler offset. The rate of change of the Doppler frequency follows the profile shown in Figure 2. At zenith, the Doppler change is -550 Hz / sec. A technique to detect this time varying Doppler without demodulating the data simplifies the receiver design. This paper explores the suitability of band edge filter based FLLs for continuous phase frequency shift keyed signals.

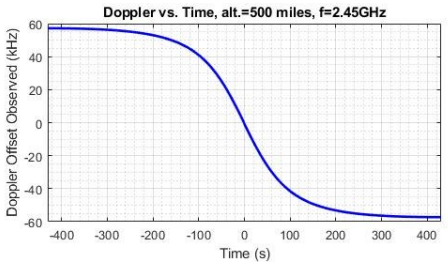

Figure 1: Doppler vs. Time (500 Mile Satellite Altitude, 2.45 GHz, overhead at time t=0)

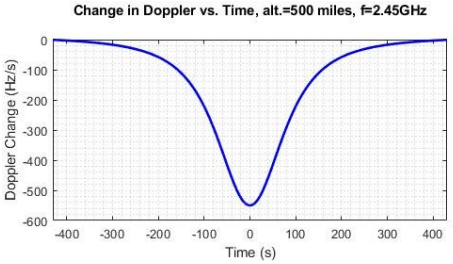

Figure 2: Change in Doppler vs. Time (500 Mile Satellite Altitude, 2.45 GHz, overhead at time t= 0)

Band Edge Filter Overview

Optimum band edge filters have a frequency response equal to the derivative with respect to frequency of the matched filter's frequency response.[1] The matched filter used to shape phase shift keyed signals is common regardless of which symbol is being transmitted, which facilitates easy implementation of the band edge FLL. In contrast, continuous-phase frequency-shift keyed (CPFSK) signals use distinct matched filters for each possible symbol. The matched filters are set equal to the time-reversed complex conjugates of the different possible symbols. A proper band edge FLL must incorporate all possible symbols into its design. The approach used in this paper will be to add the matched filters of the different possible symbols together to make a composite matched filter, denoted *g(t)*. The frequency derivative (and hence, the band edge filter prototype) is then obtained by multiplying it by *-j2πt*, employing a Fourier transform property as shown in equation (1).

$$G(f)_{BE} = \frac{\partial}{\partial f} G(f) = \int_{-\infty}^{\infty} -j2\pi t g(t) e^{-j2\pi f t} dt \quad (1)$$

The response obtained by the product *-j2πt·g(t)* contains both the upper and lower band edge portions. The time series of the individual filters is represented in equation (2), where the f_{edge} refers to the positive band edge frequency.

$$be_{upper}(t) = a(t)e^{j2\pi f_{edge} t} \quad (2)$$

$$be_{lower}(t) = b(t)e^{-j2\pi f_{edge} t}$$

It is useful to split this band edge prototype into its upper band and lower band entities because the ultimate objective is to apply them into the frequency locked loop structure shown in Figure 3. The outputs of the upper and lower band edge filters are added together to make signal cc(t) and subtracted to make signal ss(t), as shown in equation (3).

$$cc(t) = a(t)e^{j2\pi f_{edge} t} + b(t)e^{-j2\pi f_{edge} t} \quad (3)$$

$$ss(t) = a(t)e^{j2\pi f_{edge} t} - b(t)e^{-j2\pi f_{edge} t}$$

The product of cc(t) and the complex conjugate of ss(t) creates new signal with a real part equal to the difference between the upper and lower band edge filters, which is the error signal used to feed the FLL's proportional integrator filter and numerically controlled oscillator.[1] This is simple to do in the case of a binary CPFSK signal. There are only two matched filters, one for the positive frequency, one for the negative frequency. The locations of the frequencies are related to the modulation index, the ratio of the frequency separation to the symbol rate.

$$f_{edge} = \frac{h f_{sym}}{2} \quad (4)$$

In equation (4), h is the modulation index, and f_{sym} is the symbol rate. The frequencies of the two possible symbols are located at f_{edge} and $-f_{edge}$, which gives them a separation of $2f_{edge}$.

The final steps of the development are to compute the sum of the band edge filter outputs, *cc(t)*, and the difference *ss(t)*. Then, the product of *cc(t)* and the complex conjugate of *ss(t)* is computed. The real part of this product yields the energy difference between the upper and lower band edge filters. This step is shown in equation (5).

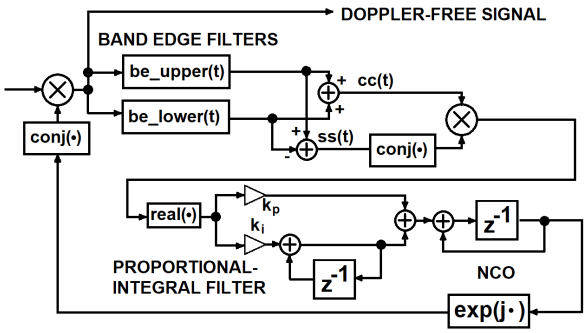

Figure 3: Band Edge FLL Design

$$cc(t) \cdot ss(t)^* = (|a(t)|^2 - |b(t)|^2) + \left(a^*(t)b(t)e^{-j2\pi 2 f_{edge} t} - a(t)b^*(t)e^{j2\pi 2 f_{edge} t}\right) \quad (5)$$

The actual matched filters in the receiver have a duration of only one symbol period, which limits the frequency resolution. If they were infinitely long, they would be represented in the frequency domain with Dirac Delta functions. Their associated band edge filters would be doublets. Finite duration matched filters have broad spectra, and the frequency derivatives broaden the spectra yet further. For example, if the modulation rate is 50 kHz, the symbol duration is 20 microseconds. Figure 4 shows how wide the matched filters and associated band edge filters are for a duration of one symbol length. It is interesting to note that in this case, the direct application of equations (3) and (5) leads to a positive band edge filter with negative frequency at equal amplitude to its intended positive frequency content. Similarly, its negative band edge filter has a positive frequency sidelobe at equal amplitude to its intended

negative frequency main lobe. This effect is caused by the fact that the matched filter positive and negative lobes are blended together to form one main lobe. In order to distinguish the distinct positive and negative matched filters, it is necessary to either increase the sample rate or increase the time duration of the filters. Figure 5 shows the effect of extending the band edge filters (and matched filter) to ten symbol durations in length. Figure 6 takes the process to the extreme, showing the spectra for 1000-symbol length filters. In each case, it can be readily observed that the peaks of the upper and lower band edge filters coincide with the spectral nulls of the composite matched filters' main lobes and sidelobes. It is also apparent that the blue and red spectra (upper and lower band edge filters) have higher sidelobes than the green (composite matched filter) spectra. This is easiest to see in Figure 5.

The trends depicted by Figure 4, Figure 5, and Figure 6 would also be true for CPFSK signals consisting of multiple bits per symbol, which would mean a larger alphabet of possible transmitted symbols. In a *M*-ary CPFSK signal, the composite matched filter has *M* tones associated with it, the upper band edge filter consists of the positive frequency matched filters, and the lower band edge filter consists of the negative frequency matched filters. As before in the binary case, the duration of the matched filters determines the bandwidth shown in the frequency domain.

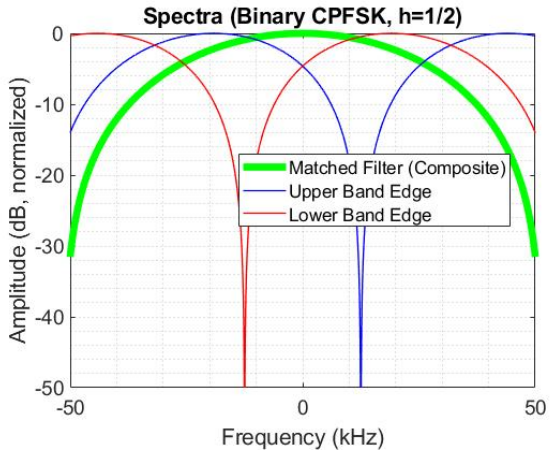

Figure 4: Matched Filter and Band Edge Filter Bandwidth (and Locations) for Binary CPFSK, h=1/2, One Symbol Length Duration

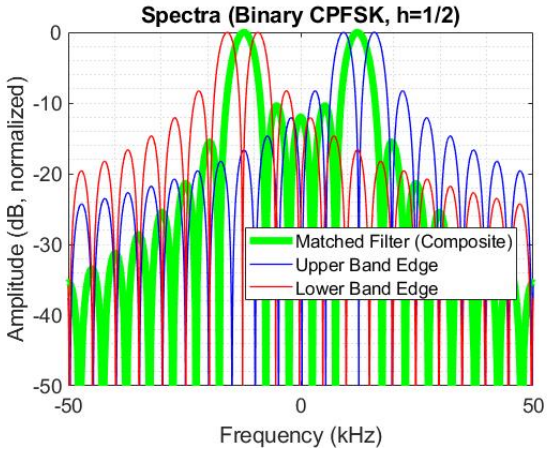

Figure 5: Matched Filter and Band Edge Filter Bandwidth (and Locations) for Binary CPFSK, h=1/2, Ten Symbol Length Duration

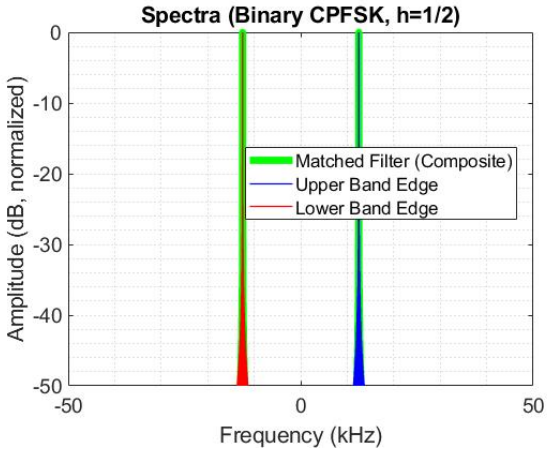

Figure 6: Matched Filter and Band Edge Filter Bandwidth (and Locations) for Binary CPFSK, h=1/2, 1000-Symbol Length Duration

CPFSK Signal Design Features Affecting Band Edge Filter Design

Whereas optimum band edge filters can be directly applied to Binary CPFSK, the application is more difficult when the number of bits per symbol is greater than 1 or when the modulation index changes from one symbol to another.

A popular design choice for CPFSK signals is to change the modulation index from one symbol to another, usually between values less than 1 in order to keep the occupied bandwidth low and improve the trellis coding gain.[2-3] Simply alternating the modulation index between one of two possible values can change the phase transition trellis in such a way that it takes longer (more symbol periods) for the trellis to repeat itself. This effect is illustrated in Figure 7 and Figure 8. In those figures,

red paths are associated with the arrival of symbol -1, and blue paths signify the arrival of symbol +1. The trellis assumes a starting phase of zero radians. During a symbol period, the amount of phase traversed is equal to the modulation index times π times the symbol. This can be seen in equation **(6)**, where f_{edge} is the frequency associated with a symbol +1, $-f_{edge}$ is the frequency for symbol -1, T_{sym} is the duration of the symbol ($1/f_{sym}$), and `Df` is the change in phase. Equation **(6)** uses the relationship between h and f_{edge} shown in (4).

$$\Delta\varphi = \pm 2\pi f_{edge} T_{sym} = \pm \pi h \quad (6)$$

It is clear from Figure 7 that the trellis repeats after two symbol periods. Compare this to the trellis shown in Figure 8 constructed by alternating the modulation index between the values 2/8 and 3/8. This trellis repeats after four symbol periods. A deeper trellis provides a higher coding gain than a shallow trellis, much like a longer constraint length for a convolutional code.[4]

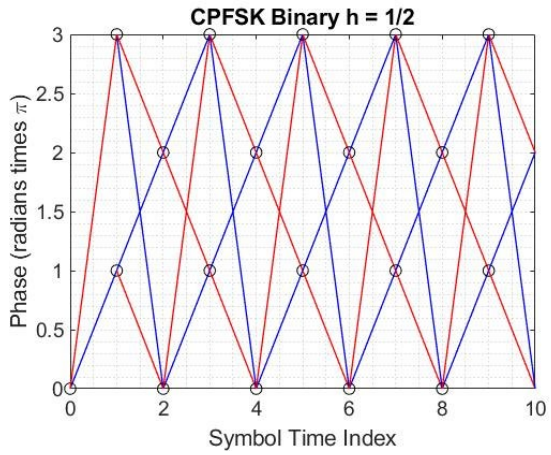

Figure 7: Trellis for Binary CPFSK, constant modulation index (h=0.5)

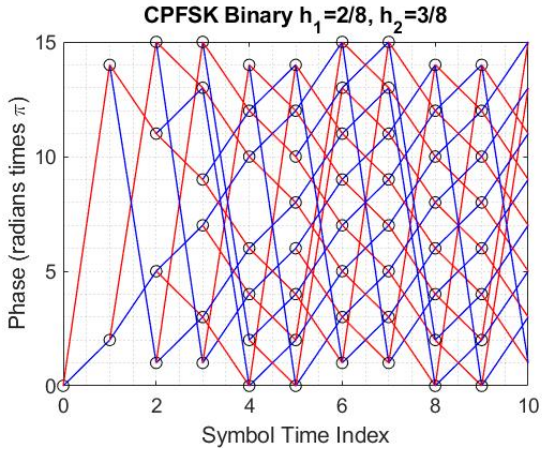

Figure 8: Trellis for Binary CPFSK, Alternating Modulation Index (h_1=2/8, h_2=3/8)

Another common choice for CPFSK signals is to use multiple bits per symbol, which expands the alphabet of symbols. The trellis of a 4-ary CPFSK signal with alternating modulation index (h_1=2/8, h_2=3/8) is shown in Figure 9. Each color represents a different symbol in the set (-3,-1,+1, +3).

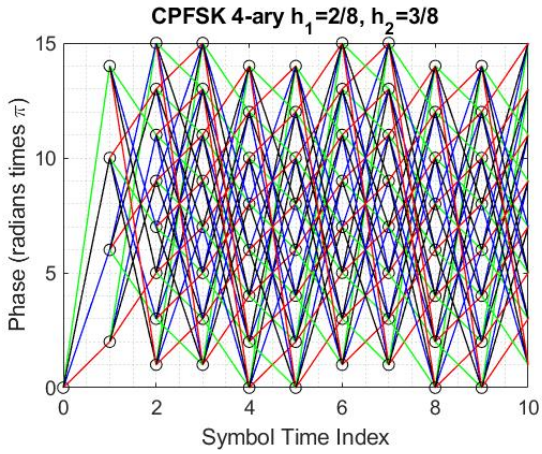

Figure 9: Trellis for 4-ary CPFSK, Alternating Modulation Index (h_1=2/8, h_2=3/8)

These design choices complicate the effort to design an optimum band edge filter for a CPFSK signal. The signal of interest itself changes frequency as a normal part of its operation, and there are multiple frequencies that it can occupy. This is especially true when the signal uses a changing modulation index. The limited time duration of the individual symbols causes the individual tones to smear into each other in the frequency domain. The direct application of the optimum band edge filter design definition from equation (1) can thus lead to spectral artifacts that prevent a clean separation between the positive and negative band edge filters.

PERFORMANCE OF OPTIMUM BAND EDGE FILTERS FOR CPFSK

Signal of Interest

The FLL from Figure 3 was tested with a 4-ary CPFSK signal with indices of modulation alternating between 2/8 and 3/8. The modulation rate was 50 kHz. A symbol is a change of frequency. For this paper, the frequency change is immediate and it occurs for a duration of one symbol. This is referred to as "full response" with rectangular shaping, or "1REC" for short.[6] This distinguishes the description of this signal from implementations that use raised cosine or other shaping filters to vary the frequency, possibly over several symbol periods ("partial response").[6]

The signal of interest was tested at signal to noise ratios of 20 dB and 5 dB. The loop parameters of the FLL, damping ratio ζ and normalized loop bandwidth η, were adjusted in order to get a combination of fast locking time and low standard deviation of error after lock. The values selected are shown in the figures to follow. The proportional and integral path coefficients from Figure 3 were computed using these values according to equation (7), which is derived in the Appendix.

$$k_p = \frac{4\zeta\eta}{1 + 2\zeta\eta + \eta^2} \qquad (7)$$

$$k_i = \frac{4\eta^2}{1 + 2\zeta\eta + \eta^2}$$

Performance of FLL with Signal Containing Time Varying Doppler Offset

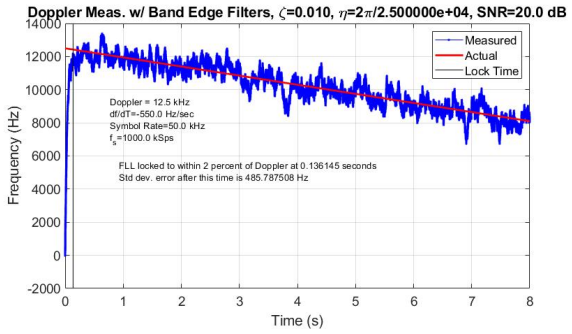

Figure 10: FLL Performance of Optimum Band Edge Filter for 4-ary CPFSK, h_1=2/8, h_2=3/8, 20 dB SNR

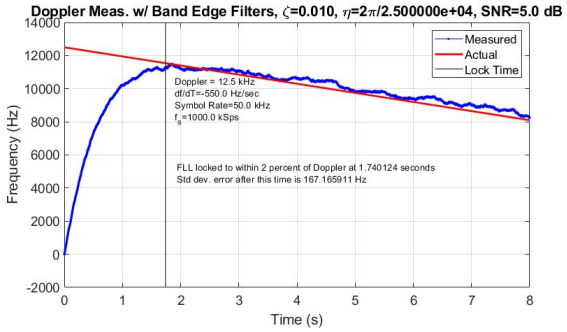

Figure 11: FLL Performance of Optimum Band Edge Filter for 4-ary CPFSK, h_1=2/8, h2=3/8, 5 dB SNR

It is interesting to note that despite having the same loop parameters ζ and η, both the 20 dB and the 5 dB SNR trials' standard deviations of error after frequency lock are comparable. However, the 5 dB trial has a lower standard deviation than the 20 dB SNR trial, although it takes longer to lock.

The slow response time in the 5 dB trial curve Figure 11 and its smoother shape when compared to the 20 dB trial curve (Figure 10) highlights an interesting interaction of CPFSK signals with band edge filters. The more noise present in the signal, the smoother the measured frequency curve. This behavior is the opposite of what is seen in band edge filter FLLs for phase shift keyed signals.[5] This effect is caused by the difference between phase and frequency shift keying. If the CPFSK signal of interest were to have a long run of the same symbol, the transmitter's modulator would output a constant frequency. The FLL receiving this signal would be reduced to functioning as an ordinary phase locked loop. In fact, the FLL has the undesired behavior of cancelling this frequency out all the way to 0 Hz rather than stopping at f_{edge}, the frequency associated with the symbol. A long run of the same symbol in a phase shift keyed signal has zero frequency content. In this case, the FLL's action of cancelling the frequency content is desirable.

What prevents the band edge FLL from cancelling out the information bearing tones in a realistic CPFSK signal is the fact that all the signals are equally likely to occur. When the signal contains changing symbols, the FLL briefly loses lock on the tone it was tracking and has to readjust. In a low SNR environment, the presence of noise causes the FLL to respond more slowly to changes in the incoming signal. This shows up as both a delayed locking time and a slow response to the normal changing of the frequency content of the signal of interest.

Performance of FLL with Signal Containing Static Doppler Offset

The signal of interest was tested with a constant 12.5kHz Doppler offset. Trials were run for 20 dB and 5 dB signal to noise ratios, and the results are shown in Figure 12 and Figure 13, respectively.

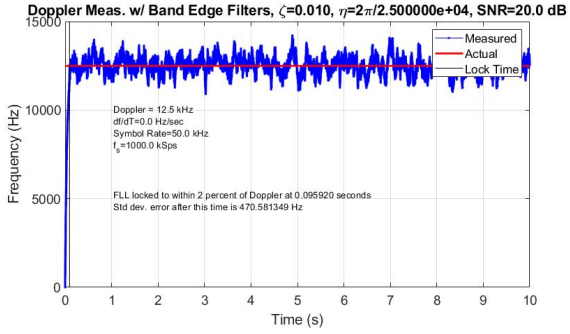

Figure 12: FLL Performance of Optimum Band Edge Filter for Static Doppler Offset, 20 dB SNR

As in the case of time-varying Doppler, these figures also show that increased noise leads to slower locking time and a lower standard deviation of error. The values of the standard deviation of error are consistent with the results for time-varying Doppler.

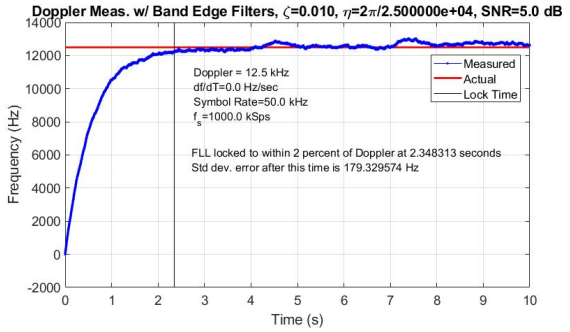

Figure 13: FLL Performance of Optimum Band Edge Filter for Static Doppler Offset, 5 dB SNR

EFFECT OF HIGH DOPPLER OFFSET ON LOW MODULATION RATE CPFSK SIGNAL

Performance of Optimum Band Edge Filters

If the modulation rate is changed from 50 kHz to 10 kHz, and the initial Doppler offset is set to 30 kHz, then the Doppler-shifted signal of interest's main lobe misses the main lobes of both of the band edge filters. The band edge filters are excited by noise in their sidelobes, and the signal of interest eventually drifts into the locking range of the FLL. Figure 14 shows an example for a 10 kHz modulated 4-ary CPFSK signal with an initial Doppler of 30 kHz, changing at a rate of -550 Hz/sec at a signal to noise ratio of 20 dB. Figure 15 shows the same scenario in 5 dB SNR. The standard deviation of error increases with decreasing SNR, and the time required to lock also increases. The standard deviation error increased for the lower SNR case because the FLL overshot the actual Doppler frequency and doesn't reverse course quickly enough to catch up.

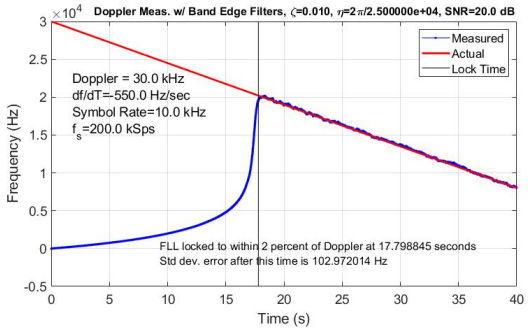

Figure 14: Performance of Optimum Band Edge Filter FLL for Time Varying Doppler Beyond Modulation Rate, 20.0 dB SNR

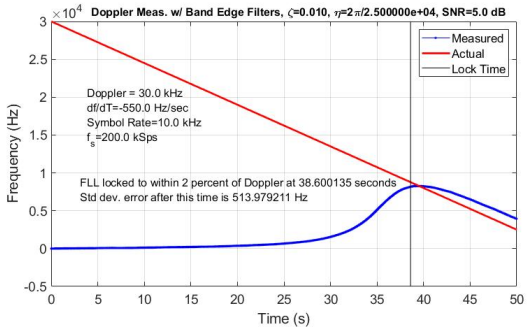

Figure 15: Performance of Optimum Band Edge Filter FLL for Time Varying Doppler Beyond Modulation Rate, 5.0 dB SNR

Alternative Design: Ramp Band Edge Filters

Instead of using the optimum design principle, a set of band edge filters was constructed using half band filters. A half band filter prototype was generated and copies were positioned at the positive and negative quarter sample rates. A ramping function was generated in the frequency domain by taking the absolute value of the ratio of frequency to sample rate. The inverse Fourier transform of this ramping function was computed and truncated to a length of 50 coefficients. This time series was then convolved with the positive and negative half band filters. The resulting sub-optimal band edge filters possess frequency slopes that emphasize high frequency offsets. When these filters are used in place of the optimum band edge design, they exhibit a better frequency lock across a wider bandwidth at the expense of having a higher standard deviation of frequency error

after lock time. The damping ratio ζ and loop parameter η had to be adjusted because of the gain of the new band edge filters.

Figure 16 shows the spectra of the half-band filter and the positive and negative band edge filters with frequency slopes. Figure 17 shows its performance in the same scenario as Figure 14, which is a 10 kHz modulation rate signal with an initial Doppler offset at 30 kHz, changing at -550 Hz/sec, in 20 dB SNR. Figure 18 is the performance of the ramp band edge FLL in the same scenario as Figure 17, except the SNR is 5 dB. Under these conditions, the ramp band edge FLL handles the high Doppler signal well. The locking time has been improved in the 20 dB case from 17.8 seconds down to .37 seconds, and in the 5 dB case from 38.6 seconds down to 5.47 seconds. The standard deviation of the frequency error after lock is comparable in both cases, but it is lower in the 20 dB trial.

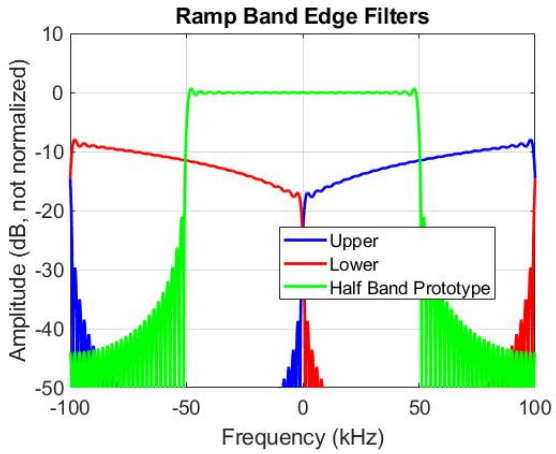

Figure 16: Spectra of Sub-optimal Band Edge Filters Created from Half Band Filters with Ramp Frequency Response

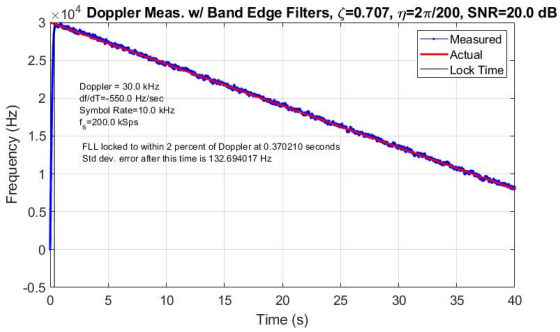

Figure 17: Performance of Ramp Band Edge Filter FLL, Initial Doppler at Three Times Modulation Rate of Signal of Interest, 20 dB SNR

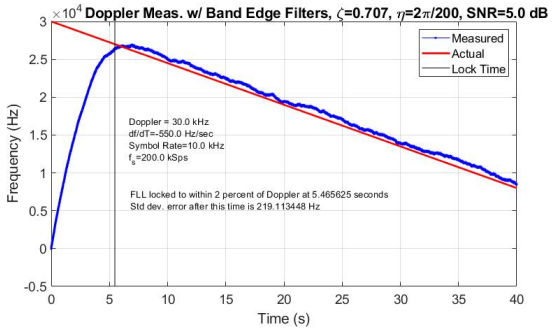

Figure 18: Performance of Ramp Band Edge Filter FLL, Initial Doppler at Three Times Modulation Rate of Signal of Interest, 5 dB SNR

The suitability of the ramp band edge filter for Doppler frequency offsets within the modulation rate needs to be explored in order to fully compare its performance to the optimum band edge filter. Figure 19 and Figure 20 show the performance of the ramp band edge FLL for a time-varying Doppler with an initial offset of 2.5 kHz (one quarter of the modulation rate) and a change of -550 Hz/sec. Figure 19 shows the 20 dB SNR trial, and Figure 20 shows the 5 dB SNR trial.

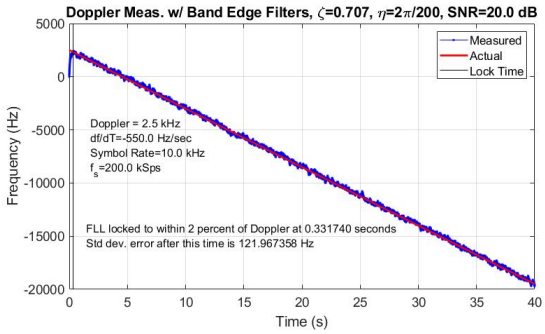

Figure 19: Performance of Ramp Band Edge Filter FLL, Initial Doppler at 1/4 of Modulation Rate of Signal of Interest, 20 dB SNR

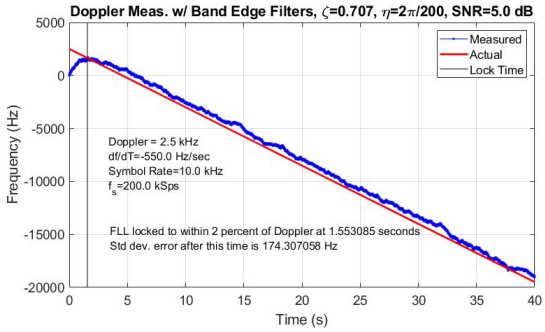

Figure 20: Performance of Ramp Band Edge Filter FLL, Initial Doppler at 1/4 of Modulation Rate of Signal of Interest, 5 dB SNR

Figure 19 is comparable to the scenario of Figure 10. Both figures have the same rate of change of Doppler (-550 Hz/sec) and the same signal to noise ratio. The ratio of the initial Doppler offset to the modulation rate is ¼ in each case. The ramp band edge filter FLL found the signal at 0.33 seconds, and had a 122 Hz standard deviation of frequency error afterward. The optimum band edge filter FLL found its signal in less than half of the time (.14 seconds), but had a larger frequency error afterwards (487 Hz). When the SNR was lowered to 5 dB, the ramp band edge FLL locked in 1.55 seconds (see Figure 20) while the optimum band edge FLL locked in 1.74 seconds (see Figure 11). However, the ramp band edge FLL has a standard deviation of frequency error (174 Hz) which is very close to the value for the optimum band edge FLL (169 Hz).

Further Refinements

In order to speed up the FLL lock time, the FLL can make use of information provided by the preamble processor in the receiver. If the NCO accumulator is initialized with an estimate of frequency before the FLL is turned on, then the FLL will be able to lock faster. Furthermore, if the preamble detector has a wider frequency search capability than the modulation bandwidth, then the FLL does not need to use ramp band edge filters to acquire a high frequency offset signal, and simple optimum band edge filters will work.

CLOSING REMARKS

Band edge filters for CPFSK signals can be implemented from the known alphabet of tones of the signal of interest. Design variations for damping ratio and loop bandwidth balance the trade-off between response time and error after lock. The authors found that a ramp band edge FLL can perform comparably to the optimum band edge FLL in situations where the Doppler offset is within the modulation bandwidth. The ramp band edge FLL outperforms the optimized band edge FLL when the signal of interest has a frequency offset beyond the main lobes of the optimum band edge filters. Furthermore, the ramp band edge FLL does not need knowledge of the CPFSK signal of interest, whereas the optimum band edge filters have to be constructed from the symbol matched filters multiplied by time vectors. The optimum band edge filter designs must be altered if the alphabet size, modulation rate, or index of modulation is changed.

APPENDIX

A stable second-order analog phase-locked loop has a denominator with the structure shown in (A.1).

$$\frac{\theta_o(s)}{\theta_i(s)} = \frac{numerator}{s^2+2\zeta\omega_n s+\omega_n^2} \tag{A.1}$$

The digital phase-locked loop with proportional constant k_p and integral constant k_i has a block diagram shown in Figure 21 and a transfer function as expressed in (A.2).

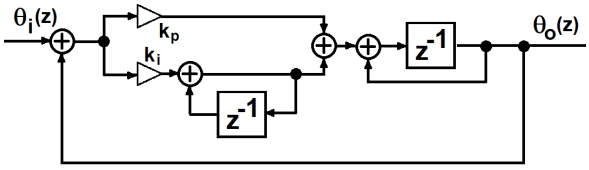

Figure 21: Second Order Digital Phase Locked Loop

$$\frac{\theta_o(z)}{\theta_i(z)} = \frac{(k_p+k_i)z-k_p}{z^2+(k_p+k_i-2)z+(1-k_p)} \tag{A.2}$$

In this derivation, the goal is to find a relationship between the proportionality constants k_p and k_i, the analog damping factor ζ, and the natural damping frequency ω_n. Our starting point is to replace the denominator of the analog system of (A.1) with an equivalent digital domain expression. The bilinear transform relating s to z is shown in (A.3).

$$s = \frac{2}{T_s}\left(\frac{z-1}{z+1}\right) \tag{A.3}$$

In (A.3), the sample period is T_s. Substituting the bilinear transform expression into (A.1) produces a new expression in terms of z as shown in (A.4).

$$\frac{\theta_o(z)}{\theta_i(z)} = \frac{numerator}{\left(\frac{z-1}{z+1}\right)^2+2\zeta\left(\frac{\omega_n T_s}{2}\right)\left(\frac{z-1}{z+1}\right)+\left(\frac{\omega_n T_s}{2}\right)^2} \tag{A.4}$$

Replacing the ratio $\omega_n T_s/2$ with η and multiplying the numerator and denominator by $(z+1)^2$, yields (A.5).

$$\frac{\theta_o(z)}{\theta_i(z)} = \frac{numerator}{(z-1)^2+2\zeta\eta(z+1)(z-1)+\eta^2} \tag{A.5}$$

Next, we combine powers of z in the denominator of (A.5) and compare the result to (A.2).

$$\frac{\theta_o(z)}{\theta_i(z)} = \frac{numerator}{z^2+z\left(\frac{2\eta^2-2}{1+2\zeta\eta+\eta^2}\right)+\left(\frac{1-2\zeta\eta+\eta^2}{1+2\zeta\eta+\eta^2}\right)} \tag{A.6}$$

Comparing (A.6) to (A.2), produces two equations with two unknowns:

$$1-k_p = \frac{1-2\zeta\eta+\eta^2}{1+2\zeta\eta+\eta^2} \tag{A.7}$$

$$k_p+k_i-2 = \frac{2\eta^2+2}{1+2\zeta\eta+\eta^2}$$

Solving (A.7) for k_p and k_i completes the derivation, with the result in (A.8)

$$k_p = \frac{4\zeta\eta}{1+2\zeta\eta+\eta^2} \quad \text{(A.8)}$$

$$k_i = \frac{4\eta^2}{1+2\zeta\eta+\eta^2}$$

Acknowledgments

The authors wish to acknowledge NIWC Pacific's Naval Innovative Science and Engineering (NISE) program committee for its continuing supporting for the project that led to this paper.

References

1. Harris, F., "Band Edge Filters: Characteristics and Performance in Carrier and Symbol Synchronization," Proceedings of the 13th International Symposium on Wireless Personal Multimedia Communications, Recife, Brazil, October 11-14, 2010.
2. Mazur, Brian A. and Desmond P. Taylor, "Demodulation and Carrier Synchronization of Multi-h Phase Codes," IEEE Transactions on Communications, vol. COM-29, No. 3, March 1981.
3. Premji, Al-Nasir and Desmond P. Taylor, "A Practical Receiver Structure for Multi-h CPM Signals," IEEE Transactions on Communications, vol. COM-35, No. 9, September 1987.
4. Forney, G. David, "The Viterbi Algorithm," Proceedings of the IEEE, vol. 61, No. 3, March 1973.
5. Hill, Brendan and Nazia Mozaffar and Salwan Damman, "A Comparison of Techniques for Non Data-Aided Carrier Tracking of Phase-Modulated Signals", Small Satellite Conference, Logan UT, August 2020.
6. Hosseini, Ehsan and Erik Perrins, "Timing, Carrier, and Frame Synchronization of Burst-Mode CPM," IEEE Transactions on Communications, vol. 61, No. 12, December 2013.